Liquid-crystal-based topological photonics

Abbaszadeh, H.; Fruchart, M.S.; Saarloos, W. van; Vitelli, V.

Liquid-crystal-based topological photonics

Hamed Abbaszadeh[a], Michel Fruchart[b,c], Wim van Saarloos[a], and Vincenzo Vitelli[b,c,d,1]

[a]Instituut-Lorentz, Universiteit Leiden, Leiden 2300 RA, The Netherlands; [b]James Franck Institute, University of Chicago, Chicago, IL 60637; [c]Department of Physics, University of Chicago, Chicago, IL 60637; and [d]Kadanoff Center for Theoretical Physics, University of Chicago, Chicago, IL 60637

Edited by David A. Weitz, Harvard University, Cambridge, MA, and approved December 14, 2020 (received for review October 6, 2020)

Liquid crystals are complex fluids that allow exquisite control of light propagation thanks to their orientational order and optical anisotropy. Inspired by recent advances in liquid-crystal photopatterning technology, we propose a soft-matter platform for assembling topological photonic materials that holds promise for protected unidirectional waveguides, sensors, and lasers. Crucial to our approach is to use spatial variations in the orientation of the nematic liquid-crystal molecules to emulate the time modulations needed in a so-called Floquet topological insulator. The varying orientation of the nematic director introduces a geometric phase that rotates the local optical axes. In conjunction with suitably designed structural properties, this geometric phase leads to the creation of topologically protected states of light. We propose and analyze in detail soft photonic realizations of two iconic topological systems: a Su–Schrieffer–Heeger chain and a Chern insulator. The use of soft building blocks potentially allows for reconfigurable systems that exploit the interplay between topological states of light and the underlying responsive medium.

topological matter | liquid crystals | metamaterials | topological photonics

Liquid crystals are soft-matter phases characterized by their orientational order (1). As a result of this order, liquid crystals can control the propagation of light in a reconfigurable way, with applications ranging from liquid-crystal displays (2) to adaptive lenses (3). In this article, we discuss how nematic liquid crystals can be used as a soft-matter platform to realize the building blocks of topological photonic materials (4–6). Topological materials are a class of structured materials exhibiting remarkable features, such as the existence of chiral edge states topologically protected against backscattering. The robustness of these edge states can be traced to the existence of topological invariants characterizing how waves propagate in the bulk of the material. Such materials, inspired by topological insulators (TIs) (7), are ubiquitous, including examples in photonics (4–6, 8–14), mechanics (15–20), hydrodynamics (21–24), stochastic systems (25), and electrical circuits (26–28). The unique properties of topological photonic materials suggest several potential applications (4–6), ranging from high-power single-mode lasers (29, 30) to slow light (31).

Here, we develop a strategy purely based on liquid crystals, where the orientation of the nematic molecules, described by their director field, is used both to realize waveguiding (32–34) and to build topological materials (10, 35, 36) by coupling these waveguides. Our proposal is inspired by recent advances in liquid-crystal technology that make it possible to effectively print out any target director field either by stacking two-dimensional photoaligned slices (32, 37–42) or through three-dimensional photopatterning techniques (43). Electrically controlled and light-driven liquid crystals (39, 44) could be further exploited to engineer reconfigurable topological photonic devices (14).

To facilitate experimental investigations of these phenomena, we develop a tight-binding (TB) model (i.e., a coupled-mode description) for the coupled liquid-crystal waveguides (45). We establish its domain of validity through a careful comparison with direct simulations of Maxwell equations. Along with a precise analysis of the symmetries in the system, these results allow us to engineer a liquid-crystal realization of two archetypal topological systems. The first is perhaps the simplest TI: an analogue of the Su–Schrieffer–Heeger (SSH) model (36, 46), which is a one-dimensional system displaying nonvanishing winding numbers. The second and more challenging one is inspired by the quantum Hall effect: an analogue of the Haldane model (47), which is a two-dimensional system with nonvanishing topological invariants called Chern numbers.

The main challenge in realizing the two-dimensional Haldane model in classic systems lies in the requirement that time-reversal (TR) symmetry must be broken (7). In electronic systems, this symmetry breaking can easily be obtained via a static magnetic field. This is more difficult in classic systems, such as photons or phonons, because of the absence of a direct coupling with the magnetic field (48–50). Here, one of the spatial directions is treated as time. More precisely, the evolution of light waves along the paraxial direction z (i.e., at small angles with the direction of propagation) can be mapped to the evolution in time t of a quantum wavefunction described by the Schrödinger equation. In this picture, modulations of the waveguide in the paraxial direction correspond to a time-dependent quantum potential (51, 52), effectively allowing TR symmetry breaking in static liquid-crystal textures.

Liquid crystals have long served as a natural laboratory to develop theoretical ideas at the interface between quantum and soft matter (11, 53–61). For instance, in de Gennes' seminal study on the analogy between smectic liquid crystals and superconductors, the spatial direction perpendicular to the smectic layer is also mapped to the time axis of a superconductor coupled to a gauge field (54–56). (In the smectic, the gauge field can be traced to the bending distortions of the layers.) More recently, variations on this space–time mapping have been exploited outside of liquid crystals to realize topological photonic states (5, 10, 62–64), in which the necessary TR symmetry breaking is obtained by breaking space-inversion symmetry ($z \to -z$). Experimental studies have unambiguously demonstrated that periodic

Significance

Liquid crystals are complex fluids that combine a unique ability to manipulate light with the reconfigurability of soft materials. They are at the core of modern display technology. Here, we suggest that nematic liquid crystals can also be used as building blocks of topological materials key to realize protected unidirectional waveguides, sensors, and lasers. Building on recent advances in liquid-crystal technology, we propose that suitable spatial modulations of the nematic director field are sufficient to assemble topological photonic materials. These ideas pave the way for fully reconfigurable photonic devices based on topologically protected states.

Author contributions: H.A., M.F., W.v.S., and V.V. designed research, performed research, analyzed data, and wrote the paper.

The authors declare no competing interest.

This article is a PNAS Direct Submission.

[1]To whom correspondence may be addressed. Email: vitelli@uchicago.edu.

This article contains supporting information online at https://www.pnas.org/lookup/suppl/doi:10.1073/pnas.2020525118/-/DCSupplemental.

Published January 20, 2021.

modulations induced by helix-shaped waveguides allow one to implement photonic Floquet TIs, a particular class of TIs in which the system is periodically driven in time (10). In these helix-shaped waveguides, the change in the local direction of propagation leads to geometric phases (65, 66) called Rytov–Vladimirskii–Berry phases (67, 68), which are eventually responsible for the existence of the photonic TI. Our system displays different geometric phases from ref. 10: the so-called Pancharatnam–Berry phases (69, 70) that stem from the change in the local optical axes.

A distinctive feature of our liquid-crystal system is that the symmetries of the photonic topological material can be entirely controlled by the spatial symmetries of the nematic texture, a point of considerable interest for topological engineering applications. Not only does the patterned nematic allow for an effective TR symmetry breaking, but it also generates the soft waveguides that are the building blocks of our topological materials. Unlike permanent waveguides embedded in a composite material, these soft waveguides could be switched on and off by applying suitable external fields that induce the necessary nematic textures.

Light Confinement via Periodic Drive.

Consider the propagation of a Gaussian light beam in a uniform nematic liquid crystal, where the nematic rods are in the plane orthogonal to the direction of propagation. Because of the shape of the nematic molecules, beams with different polarizations experience different refractive indices. The medium is characterized by two particular indices, n_o and n_e, that correspond to the so-called ordinary and extraordinary polarizations that propagate unchanged. Hence, three characteristic length scales naturally appear: the light wavelength λ, the beating length $\Lambda = \lambda/(n_e - n_o)$ between the ordinary and extraordinary polarizations, and the Rayleigh length Z_R that determines the size of the Gaussian beam. Additional length scales characterize the spatial pattern of the liquid crystal. Here, we focus on patterns where only the orientation of the nematic liquid-crystal molecules (i.e., the director field) is changed, while the ordinary and extraordinary indices n_o and n_e are the same in the whole system. This orientation is determined by the angle $\theta(x, y, z)$ that the rod-like molecules make with the y axis, as shown in Fig. 1*A*. In the regime where $Z_R \gg \Lambda, \lambda$, the dynamics of the electromagnetic field can effectively be described by the evolution of a slowly varying wavepacket ψ, which is a two-component vector in the polarization space. In the paraxial approximation, the evolution of this wavepacket is described by (10, 32, 51, 52)

$$i\,\frac{\partial \psi}{\partial z} = -\frac{1}{2\bar{n}k_0}\,[\nabla_\perp + i\mathrm{A}]^2\psi + \mathrm{V}\psi, \qquad [1]$$

with the synthetic gauge field $\mathrm{A}(z) = -(\nabla_\perp\theta)\mathrm{S}(z)$ and the potential $\mathrm{V}(z) = -(\partial_z\theta)\mathrm{S}(z)$, where $\mathrm{S}(z)$ is a z-dependent matrix that only depends on Λ and is responsible for the polarization dynamics (*SI Appendix*). Formally, this equation resembles the Schrödinger equation of quantum mechanics, provided that the paraxial direction z is replaced by time.

When the orientation $\theta(x, y, z)$ of the director field is periodic in the paraxial direction z with a period Λ, the Hamiltonian is Λ-periodic in z and can be analyzed by using Floquet theory (71, 72). The main idea is that the propagation of light over large distances $z \gg \Lambda$ is essentially captured by repeating its evolution over one period Λ, which is described by the evolution operator $U(\Lambda)$ associated with Eq. **1**. The eigenvalues of the operator $U(\Lambda)$ are phases of the form $e^{-i\kappa\Lambda}$, where κ is the quasi-momentum in the paraxial direction of the corresponding eigenmode. Here, the eigenmodes describe guided modes of the soft waveguide (32), and, up to variations at the (small) scale of the period Λ, their intensity remains constant.

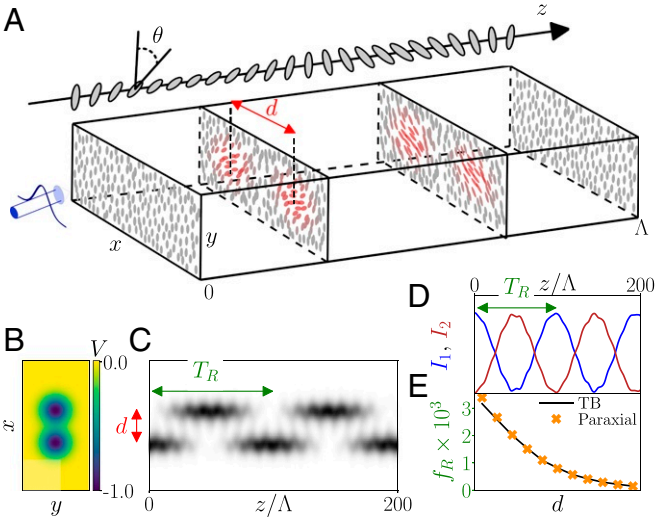

Fig. 1. Coupling of two waveguides, corresponding to the liquid-crystal pattern in *A* and with an effective optic potential shown in *B*. The *z* axis in *A* shows the orientation of the molecules in the center of a waveguide for one Floquet period, given by Λ. (*C* and *D*) The intensity profile obtained with the guided mode of one of the waveguides as an initial condition shows an oscillatory pattern, which is reminiscent of Rabi oscillations in two-level quantum systems. (*E*) Dependence of the dimensionless Rabi frequency $f_R = \lambda/T_R$ with the distance between waveguides for both the continuum paraxial simulations and the TB method. The effective coupling between two such waveguides, proportional to f_R, decays exponentially with their distance.

Coupling of Waveguides

We now consider a system that consists of two such soft photonic waveguides by transversely repeating the director modulation which corresponds to one waveguide (Fig. 1*A*). When two of these waveguides are located close to each other, they become coupled, as light can tunnel from a waveguide to another through evanescent waves: the electromagnetic field inside one waveguide induces a field inside the other one. Fig. 1*C* shows that if a guided mode is initially inside one of the two identical waveguides, it will eventually leak into the other one. The light-intensity pattern obtained from this coupling oscillates sinusoidally with a period T_R (Fig. 1*D*) exactly like Rabi oscillations in two-level quantum systems. We confirm these results by directly solving the full Maxwell equations with the finite-difference time-domain method using the open-source software package MEEP (73).

We wish to consider a system made of a large number of coupled waveguides. To do so, we need a simplified description of the waveguides and of their couplings that allows to capture the essential features of the system (such as the Rabi oscillations described above) without having to describe the full liquid-crystal configuration. Hence, we use a time-dependent Hückel method (74, 75) to develop a TB model for the photonic waveguides (*SI Appendix*). The TB Hamiltonian H^{TB} obtained by using this method for the evolution of a system of N waveguides reads

$$i\partial_z\,|\psi_n\rangle = \sum_{m=1}^{N} H^{\mathrm{TB}}_{nm}(z)\,|\psi_m\rangle\,, \qquad [2]$$

where ψ_n is the mode inside waveguide n. This TB model brings the essential simplicity that is needed to analyze a system with many coupled waveguides, such as a lattice configuration. The Rabi oscillations obtained from this TB model for a two-waveguide system are in agreement with the solutions of the Schrödinger Eq. **1** in the continuum using appropriate initial conditions, validating our approach (Fig. 1*E*). Using this TB

model, we further quantify the coupling between two waveguides and observe that the coupling strength decays exponentially with respect to the distance between the waveguides (Fig. 1*E*)

Photonic Crystals in 1+1d: SSH Chain. A lattice of coupled waveguides is obtained by a periodic patterning of the nematic director in the transverse plane. Here, we consider a 1+1d lattice, where the second dimension stands for the paraxial direction z that plays the role of time in this system. We consider a system inspired by the SSH model (36, 46). Using the coupling-distance dependence from the section *Coupling of Waveguides*, we design a lattice of these waveguides on a chain so that the coupling between two neighboring waveguides changes in an alternating way, as shown in Fig. 2 *A* and *B*. The distance between waveguides is chosen such that the ratio between the two different hopping amplitudes is $J_-/J_+ = 0.25(1)$.

Fig. 2 *A* and *B* also shows that, depending on the ordering of the strong and weak bonds at the boundary, there are two different dimerizations of the neighboring waveguides. The TB description of the system in Fig. 2 *A* and *B* is a time-dependent version of the SSH chain (46). We find a photonic state that remains at the edge of one of the two configurations of this system, as shown in Fig. 2*C*, whereas in the other configuration, in Fig. 2*D*, the initial mode at the edge leaks into the bulk while it propagates forward. The intensity profile of the localized edge mode shows an exponential decay away from the waveguide at the boundary. The presence of this edge mode is due to the topology of the Hamiltonian describing the system, which is characterized by an integer winding number across the Brillouin zone (BZ) (*SI Appendix*). In this particular case, this topological invariant depends on whether J_- is smaller or greater than J_+, which explains why this edge mode is present in only one of the two configurations in Fig. 2.

Symmetries and Topological Modes in 2+1d

So far, we only considered systems in which there is a symmetry between the photonic modes that propagate forward and backward along the z direction. This z-reversal symmetry corresponds to TR symmetry in the effective quantum picture. We would now like to explore the phenomena that can arise with introducing an asymmetry in this direction. The TR symmetry acts on Eq. **1** through the operator $T = \sigma_z \Theta$, where Θ is complex conjugation and where the Pauli matrix σ_z exchanges right and left circular polarizations. It follows that a configuration is TR-invariant if there is a reference point z_0 such that the orientation of the directors satisfies $\theta(z_0 - z) = -\theta(z_0 + z)$ (*SI Appendix*). In the TB model of this system, we focus on the subspace of guided modes, since the unguided ones do not follow a coupled-mode picture. In this reduced description, the TR operator is simply the complex conjugation operator Θ. We prove analytically in *SI Appendix* that the TR invariance in the paraxial Hamiltonian leads to the TR invariance of the TB model.

We break TR symmetry by considering the director-field configuration

$$\theta(x, y, z) = \theta_0(x, y)\,[\sin \Omega z + \eta\, \cos(2\Omega z - \varphi)], \qquad [3]$$

where $\theta_0(x, y)$ describes the nematic pattern in the transverse plane (it is a sum of Gaussians centered at desired positions), $\Omega = 2\pi/\Lambda$ is the frequency of the drive (an inverse length scale here), η is a dimensionless coefficient that controls the strength of the TR symmetry breaking, and φ is the dephasing between the harmonics of the pattern. We focus on configurations of these waveguides in 2+1 dimensions, where the absence of TR invariance can lead to topological modes (5, 10, 47). A 2+1d lattice of these waveguides can be designed by considering transverse modulations of the nematic directors that are periodic in two directions. We consider a modulation that creates a honeycomb lattice of such waveguides in the transverse plane, as shown in Fig. 3*A*.

We find that in our Floquet model, the TR symmetry breaking is not sufficient to get a topological band structure. This can be understood through a high-frequency Magnus expansion (71) of a general Floquet TB Hamiltonian on a honeycomb lattice, by mapping the obtained effective Hamiltonian to the Hamiltonian of the Haldane model (47) (*SI Appendix*). We find that breaking the threefold symmetry between the three neighboring bonds is necessary to get a nonzero Haldane mass at the first order of the expansion. Many Floquet-driven models involve a rotating gauge field, arising, for example, from the coupling with a circularly polarized light radiation (76) or an effective gauge field originating from spin-orbit coupling of light on a helical waveguide (10). In this case, the rotating gauge field effectively breaks the C_3 symmetry via a Peierls substitution in the hoppings.

Here, we do not have access to such a rotating gauge field. Instead, we break this symmetry by shifting the waveguides along the z axis, with a shift that is different for each of the neighboring waveguides (Fig. 3*B*). The relative shift of waveguides affects both the strength of their couplings, as shown in Fig. 3*C*, and induces a dephasing between the hoppings. We choose a spatially periodic configuration of phase shifts. However, the unit cell is enlarged with respect to the hexagonal lattice, as shown in Fig. 3*B*, where the colors represent the shifts.

We note that the TB description is only reliable when the shifts are small enough (Fig. 3*C*). We use the guided mode of each waveguide as a basis for the TB description. This works well when the waveguides are not shifted. When they are, our procedure does not span the whole space where the modes evolve when the waveguides are shifted, because the guided modes of waveguides with relative shifts are different: The guided mode of one waveguide can be repelled from a similar waveguide with a relative shift of origin. In the following, we focus on the range of shifts where the TB description still provides a reliable approximation (blue dashed rectangle in Fig. 3*C*).

The band structures associated with the TB model of the lattices of waveguides in Fig. 3 *A* and *B* on a cylinder are shown in Fig. 3 *E* and *F*. Fig. 3*E* corresponds to a honeycomb lattice of

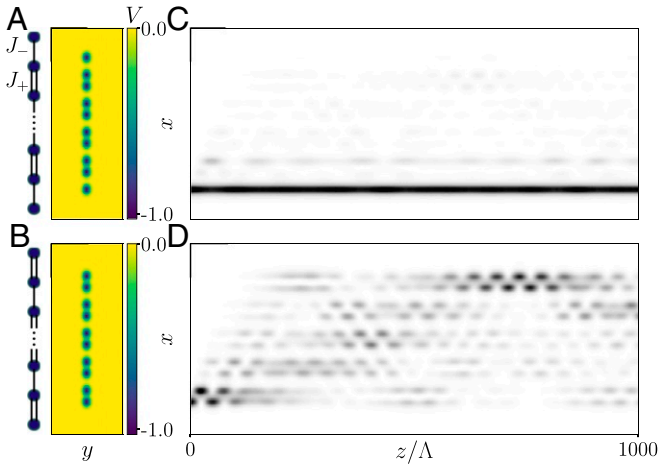

Fig. 2. An SSH chain of photonic waveguides in a liquid-crystal medium. (*A* and *B*) The effective photonic potential for two topologically distinct dimerizations of the waveguides in such system, which correspond to a SSH chain with and without an edge mode, respectively, as shown in *C* and *D*. The effective tunneling between these waveguides is controlled by their distance, as illustrated in Fig. 1*E*. *A* and *B*, *Insets* sketch an SSH chain corresponding to each system. Strong (J_+) and weak (J_-) couplings are shown by double and single bonds, respectively. (*C*) The propagation of an edge mode whose existence is topologically protected. (*D*) The scattering into the bulk of the same initial mode in a trivial chain.

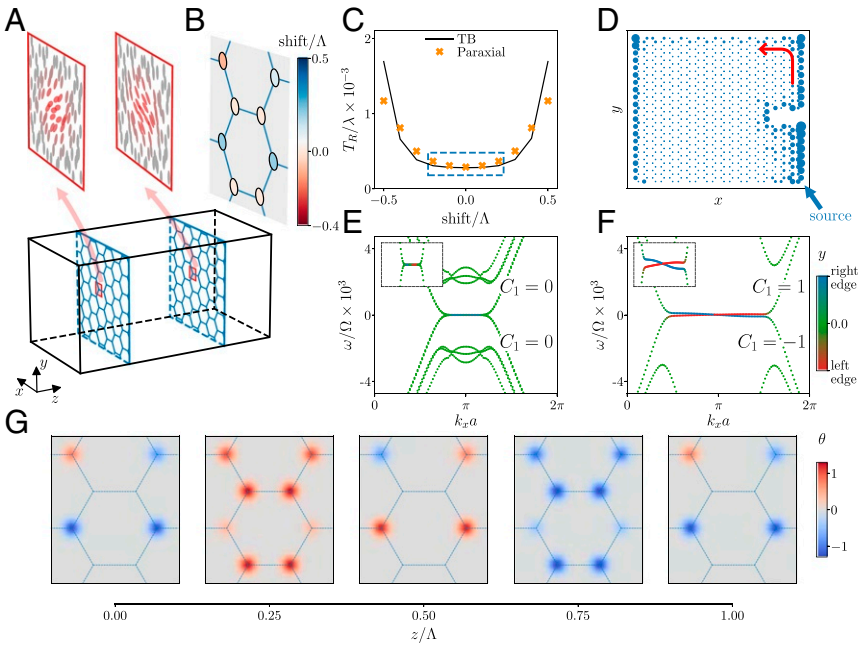

Fig. 3. (*A*) A photonic lattice on a honeycomb structure that is obtained by patterning of the nematic directors in the transverse plane. Each node of the lattice corresponds to a photonic waveguide, as shown in the zoomed-in panels. (*B*) A unit cell of this photonic lattice, where the waveguides are colored according to their relative phase shift in the z direction. The unit cell is enlarged with respect to the honeycomb one because of the different phase shifts. (*C*) The Rabi period between two photonic waveguides as a function of the relative shift between them. We focus on the parameter space enclosed by the blue dotted rectangle, where there is a close agreement between the TB model and the continuum paraxial simulations. (*D*) Evolution of a topological edge mode on the projected $x-y$ plane. The size of each circle corresponds to the light intensity on that site. This mode propagates along the edge without backscattering on obstacles. The propagation direction of this edge mode is depicted with a red arrow. (*E* and *F*) One sideband in the Floquet band structure of a honeycomb lattice of photonic waveguides without (*E*) and with (*F*) relative phase shift. In both cases, the TR symmetry is violated using the structural parameter $\eta = 0.67$. The band structure in *F* shows the presence of one mode at the right (blue) and left (red) edge of this system for a range of transverse momenta in the BZ. The presence of these edge modes and their unidirectional propagation are predicted by the difference between first Chern numbers C_1 of the bands, which are separated by the gap. (*G*) Snapshots of the director-field configuration in the unit cell shown in *B* during one Floquet period. Gray areas correspond to regions where the directors are along the y direction.

waveguides without relative phase shifts. Fig. 3*F* corresponds to the unit cell shown in Fig. 3*B*, where the waveguides are shifted with respect to each other. In this case, we observe chiral modes localized at the edges of the cylinder. A direct calculation of the first Chern number of the top and bottom bands (*SI Appendix*) shows that these edge modes have a topological origin. They circulate unidirectionally along the edge in the transverse plane as they propagate along the z direction, despite the presence of a defect at the boundary (Fig. 3*D*) The decay length of the edge modes in the bulk is related to the inverse size of the bulk band gap in which these modes reside, compared to the frequency of the Rabi oscillation. Thus, we find that the decay length is only a few lattice sites, even though the gap is very small with respect to the Floquet frequency.

Non-Hermitian Description of Shifted Waveguides

A full description of the photonic crystal should encompass both guided and repelled modes. The analysis above shows that waveguides shifted with respect to each other can be coupled. In this situation, both the guided and repelled modes should be taken into account. In principle, this would entail the use of a non-Hermitian Hamiltonian (77) to describe the system, to account for the loss of light intensity due to the repelled light (eventually converted to heat in the bulk of the material). We have verified that non-Hermitian effects involving nonorthogonal eigenmodes are negligible in the topological system described in *Symmetries and Topological Models in 2+1d*, validating our approach based on Hermitian topological invariants. Looking forward, the natural occurrence of non-Hermiticity in the description suggests liquid-crystal-based soft waveguides as a promising platform for non-Hermitian optics (78–81).

Conclusion

In this work, we have shown how to realize photonic Floquet topological systems using liquid crystals. As an example, we have shown how Floquet versions of the SSH and Haldane models can be realized. As photonic crystals, these photonic Floquet TIs are semimetal phases with a strong anisotropy; for instance, a $(2+1)$ -dimensional Chern insulator can be seen as a photonic Weyl material (82, 83). Our analysis based on a reduction of the paraxial wave equation to a TB description provides a blueprint to design photonic structures with targeted topological properties in liquid crystal systems through Pancharatnam–Berry phases.

Data Availability. There are no data underlying this work.

ACKNOWLEDGMENTS. This work was primarily supported by the University of Chicago Materials Research Science and Engineering Center, which is funded by National Science Foundation under Award no. DMR-2011854. H.A. and M.F. (earlier position in Leiden) were supported by the Foundation for Fundamental Research on Matter (FOM) and the Netherlands Organization for Scientific Research (NWO). V.V. was supported by the Simons Foundation; and Complex Dynamics and Systems Program of the Army Research Office Grant W911NF-19-1-0268. M.F. acknowledges support from an MRSEC-funded Kadanoff-Rice fellowship (DMR-2011854). We thank Oleg Lavrentovich for discussions.

1. P. G. De Gennes, J. Prost, *The Physics of Liquid Crystals* (Oxford University Press, Oxford, UK, 1993).

2. H. Kawamoto, The history of liquid-crystal displays. *Proc. IEEE* **90**, 460–500 (2002).

3. J. F. Algorri, D. C. Zografopoulos, V. Urruchi, J. M. Sánchez-Pena, Recent advances in adaptive liquid crystal lenses. *Crystals* **9**, 460–500 (2019).
4. L. Lu, J. D. Joannopoulos, M. Soljačić, Topological photonics. *Nat. Photon.* **8**, 821–829 (2014).
5. T. Ozawa *et al.*, Topological photonics. *Rev. Mod. Phys.* **91**, 015006 (2019).
6. M. S. Rider *et al.*, A perspective on topological nanophotonics: Current status and future challenges. *J. Appl. Phys.* **125**, 120901 (2019).
7. M. Z. Hasan, C. L. Kane, Colloquium: Topological insulators. *Rev. Mod. Phys.* **82**, 3045–3067 (2010).
8. M. Hafezi, S. Mittal, J. Fan, A. Migdall, J. M. Taylor, Imaging topological edge states in silicon photonics. *Nat. Photon.* **7**, 1001–1005 (2013).
9. A. B. Khanikaev *et al.*, Photonic topological insulators. *Nat. Mater.* **12**, 233–239 (2013).
10. M. C. Rechtsman *et al.*, Photonic floquet topological insulators. *Nature* **496**, 196–200 (2013).
11. M. Fruchart *et al.*, Soft self-assembly of Weyl materials for light and sound. *Proc. Natl. Acad. Sci. U.S.A.* **115**, E3655–E3664 (2018).
12. J. Yuen-Zhou, S. K. Saikin, N. Y. Yao, A. Aspuru-Guzik, Topologically protected excitons in porphyrin thin films. *Nat. Mater.* **13**, 1026–1032 (2014).
13. J. Yuen-Zhou *et al.*, Plexciton Dirac points and topological modes. *Nat. Commun.* **7**, 11783 (2016).
14. M. I. Shalaev, S. Desnavi, W. Walasik, N. M. Litchinitser, Reconfigurable topological photonic crystal. *New J. Phys.* **20**, 023040 (2018).
15. L. M. Nash *et al.*, Topological mechanics of gyroscopic metamaterials. *Proc. Natl. Acad. Sci. U.S.A.* **112**, 14495–14500 (2015).
16. R. Süsstrunk, S. D. Huber, Observation of phononic helical edge states in a mechanical topological insulator. *Science* **349**, 47–50 (2015).
17. S. H. Mousavi, A. B. Khanikaev, Z. Wang, Topologically protected elastic waves in phononic metamaterials. *Nat. Commun.* **6**, 8682 (2015).
18. S. D. Huber, Topological mechanics. *Nat. Phys.* **12**, 621–623 (2016).
19. X. Zhang, M. Xiao, Y. Cheng, M. H. Lu, J. Christensen, Topological sound. *Commun. Phys.* **1**, 97 (2018).
20. G. Ma, M. Xiao, C. T. Chan, Topological phases in acoustic and mechanical systems. *Nat. Rev. Phys.* **1**, 281–294 (2019).
21. A. Souslov, B. C. van Zuiden, D. Bartolo, V. Vitelli, Topological sound in active-liquid metamaterials. *Nat. Phys.* **13**, 1091–1094 (2017).
22. A. Souslov, K. Dasbiswas, M. Fruchart, S. Vaikuntanathan, V. Vitelli, Topological waves in fluids with odd viscosity. *Phys. Rev. Lett.* **122**, 128001 (2019).
23. P. Delplace, J. B. Marston, A. Venaille, Topological origin of equatorial waves. *Science* **358**, 1075–1077 (2017).
24. C. Tauber, P. Delplace, A. Venaille, A bulk-interface correspondence for equatorial waves. *J. Fluid Mech.* **868**, R2 (2019).
25. A. Murugan, S. Vaikuntanathan, Topologically protected modes in non-equilibrium stochastic systems. *Nat. Commun.* **8**, 13881 (2017).
26. J. Ningyuan, C. Owens, A. Sommer, D. Schuster, J. Simon, Time- and site-resolved dynamics in a topological circuit. *Phys. Rev. X* **5**, 021031 (2015).
27. V. V. Albert, L. I. Glazman, L. Jiang, Topological properties of linear circuit lattices. *Phys. Rev. Lett.* **114**, 173902 (2015).
28. C. H. Lee *et al.*, Topolectrical circuits. *Commun. Phys.* **1**, 39 (2018).
29. G. Harari *et al.*, Topological insulator laser: Theory. *Science* **359**, eaar4003 (2018).
30. M. A. Bandres *et al.*, Topological insulator laser: Experiments. *Science* **359**, eaar4005 (2018).
31. J. Guglielmon, M. C. Rechtsman, Broadband topological slow light through higher momentum-space winding. *Phys. Rev. Lett.* **122**, 153904 (2019).
32. S. Slussarenko *et al.*, Guiding light via geometric phases. *Nat. Photon.* **10**, 571–575 (2016).
33. A. Alberucci *et al.*, "A new waveguiding mechanism based upon geometric phase," in *Frontiers in Optics 2016*. (Optical Society of America, Washington, DC, 2016), p. FF3H.3.
34. C. P. Jisha, A. Alberucci, L. Marrucci, G. Assanto, Interplay between diffraction and the Pancharatnam-Berry phase in inhomogeneously twisted anisotropic media. *Phys. Rev. A* **95**, 023823 (2017).
35. L. J. Maczewsky, J. M. Zeuner, S. Nolte, A. Szameit, Observation of photonic anomalous floquet topological insulators. *Nat. Commun.* **8**, 13756 (2017).
36. M. Bellec, C. Michel, H. Zhang, S. Tzortzakis, P. Delplace, Non-diffracting states in one-dimensional floquet photonic topological insulators. *Euro. Phys. Lett.* **119**, 14003 (2017).
37. V. Chigrinov, V. Kozenkov, H. Kwok, *Photoalignment of Liquid Crystalline Materials: Physics and Applications* (Wiley Series in Display Technology, Wiley, Chichester, UK, 2008).
38. O. Yaroshchuk, Y. Reznikov, Photoalignment of liquid crystals: Basics and current trends. *J. Mater. Chem.* **22**, 286–300 (2012).
39. H. K. Bisoyi, Q. Li, Light-driven liquid crystalline materials: From photo-induced phase transitions and property modulations to applications. *Chem. Rev.* **116**, 15089–15166 (2016).
40. Y. Guo *et al.*, High-resolution and high-throughput plasmonic photopatterning of complex molecular orientations in liquid crystals. *Adv. Mater.* **28**, 2353–2358 (2016).
41. H. Yu *et al.*, Plasmonic metasurfaces with high UV-vis transmittance for photopatterning of designer molecular orientations. *Adv. Optic. Mater.* **7**, 1900117 (2019).
42. M. Jiang *et al.*, Low f-number diffraction-limited Pancharatnam-Berry microlenses enabled by plasmonic photopatterning of liquid crystal polymers. *Adv. Mater.* **31**, 1808028 (2019).
43. T. Sasaki, H. Ono, N. Kawatsuki, Anisotropic photonic structures induced by three-dimensional vector holography in dye-doped liquid crystals. *J. Appl. Phys.* **104**, 043524 (2008).
44. A. B. Golovin, O. D. Lavrentovich, Electrically reconfigurable optical metamaterial based on colloidal dispersion of metal nanorods in dielectric fluid. *Appl. Phys. Lett.* **95**, 254104 (2009).
45. A. Yariv, Coupled-mode theory for guided-wave optics. *IEEE J. Quant. Electron.* **9**, 919–933 (1973).
46. W. P. Su, J. R. Schrieffer, A. J. Heeger, Solitons in polyacetylene. *Phys. Rev. Lett.* **42**, 1698–1701 (1979).
47. F. D. M. Haldane, Model for a quantum Hall effect without Landau levels: Condensed-matter realization of the "parity anomaly". *Phys. Rev. Lett.* **61**, 2015–2018 (1988).
48. Aidelsburger M., Nascimbene S., Goldman N., Artificial gauge fields in materials and engineered systems. *Compt. Rendus Phys.* **19**, 394–432 (2018).
49. M. C. Rechtsman *et al.*, Strain-induced pseudomagnetic field and photonic Landau levels in dielectric structures. *Nat. Photon.* **7**, 153–158 (2013).
50. H. Abbaszadeh, A. Souslov, J. Paulose, H. Schomerus, V. Vitelli, Sonic Landau levels and synthetic gauge fields in mechanical metamaterials. *Phys. Rev. Lett.* **119**, 195502 (2017).
51. S. Longhi, Quantum-optical analogies using photonic structures. *Laser Photon. Rev.* **3**, 243–261 (2009).
52. A. Szameit, S. Nolte, Discrete optics in femtosecond-laser-written photonic structures. *J. Phys. B Atom. Mol. Opt. Phys.* **43**, 163001 (2010).
53. D. R. Nelson, *Defects and Geometry in Condensed Matter Physics* (Cambridge University Press, Cambridge, UK, 2002).
54. P. de Gennes, An analogy between superconductors and smectics A. *Solid State Commun.* **10**, 753–756 (1972).
55. B. I. Halperin, T. C. Lubensky, S.-k. Ma, First-order phase transitions in superconductors and smectic-ALiquid crystals. *Phys. Rev. Lett.* **32**, 292–295 (1974).
56. P. Oswald, P. Pieranski, *Smectic and Columnar Liquid Crystals—Concepts and Physical Properties Illustrated by Experiments* (CRC Press, Boca Raton, FL, 2005).
57. R. D. Kamien, P. L. Doussal, D. R. Nelson, Theory of directed polymers. *Phys. Rev.* **45**, 8727–8750 (1992).
58. T. C. Lubensky, S. R. Renn, Twist-grain-boundary phases near the nematic–smectic-*A*–smectic-*C* point in liquid crystals. *Phys. Rev.* **41**, 4392–4401 (1990).
59. S. R. Renn, T. C. Lubensky, Abrikosov dislocation lattice in a model of the cholesteric–to–smectic-A transition. *Phys. Rev.* **38**, 2132–2147 (1988).
60. D. Z. Rocklin, P. M. Goldbart, Directed-polymer systems explored via their quantum analogs: General polymer interactions and their consequences. *Phys. Rev. B* **88**, 165417 (2013).
61. R. P. Pedro, J. Paulose, A. Souslov, M. Dresselhaus, V. Vitelli, Topological protection can arise from thermal fluctuations and interactions. *Phys. Rev. Lett.* **122**, 118001 (2019).
62. Y. E. Kraus, Y. Lahini, Z. Ringel, M. Verbin, O. Zilberberg, Topological states and adiabatic pumping in quasicrystals. *Phys. Rev. Lett.* **109**, 106402 (2012).
63. M. Verbin, O. Zilberberg, Y. Lahini, Y. E. Kraus, Y. Silberberg, Topological pumping over a photonic Fibonacci quasicrystal. *Phys. Rev. B* **91**, 064201 (2015).
64. Y. Ke *et al.*, Topological phase transitions and Thouless pumping of light in photonic waveguide arrays. *Laser Photon. Rev.* **10**, 995–1001 (2016).
65. M. V. Berry, Quantal phase factors accompanying adiabatic changes. *Proc. Math. Phys. Eng. Sci.* **392**, 45–57 (1984).
66. E. Cohen *et al.*, Geometric phase from Aharonov-Bohm to Pancharatnam-Berry and beyond. *Nat. Rev. Phys.* **1**, 437–449 (2019).
67. S. Rytov, "Transition from wave to geometrical optics. Dokl. Akad. Nauk. USSR XVIII. translated, 1938" in *Topological Phases in Quantum Theory*, S. I. Vinitsky, B. Markovski, Eds. (World Scientific, Singapore, 1989).
68. V. Vladimirskii, "The rotation of polarization plane for curved light ray. Dokl. Akad. Nauk. USSR 21. translated in 1941" in *Topological Phases in Quantum Theory*, S. I. Vinitsky, B. Markovski, Eds. (World Scientific, Singapore, 1989).
69. S. Pancharatnam, Generalized theory of interference, and its applications. *Proc. Indiana Acad. Sci.* **44**, 247–262 (1956).
70. M. Berry, The adiabatic phase and Pancharatnam's phase for polarized light. *J. Mod. Optic.* **34**, 1401–1407 (1987).
71. M. Bukov, L. D'Alessio, A. Polkovnikov, Universal high-frequency behavior of periodically driven systems: From dynamical stabilization to Floquet engineering. *Adv. Phys.* **64**, 139–226 (2015).
72. N. Goldman, J. Dalibard, Periodically driven quantum systems: Effective Hamiltonians and engineered gauge fields. *Phys. Rev. X* **4**, 031027 (2014).
73. A. F. Oskooi *et al.*, MEEP: A flexible free-software package for electromagnetic simulations by the FDTD method. *Comput. Phys. Commun.* **181**, 687–702 (2010).
74. E. Hückel, Quantentheoretische beiträge zum benzolproblem. *Z. Phys.* **70**, 204–286 (1931).
75. M. J. Ablowitz, J. T. Cole, Tight-binding methods for general longitudinally driven photonic lattices: Edge states and solitons. *Phys. Rev. A* **96**, 043868 (2017).
76. A. Gómez-León, P. Delplace, G. Platero, Engineering anomalous quantum Hall plateaus and antichiral states with ac fields. *Phys. Rev. B* **89**, 205408 (2014).
77. C. M. Bender, S. Boettcher, Real spectra in non-Hermitian Hamiltonians having PT symmetry. *Phys. Rev. Lett.* **80**, 5243–5246 (1998).
78. M. A. Miri, A. Alù, Exceptional points in optics and photonics. *Science* **363**, eaar7709 (2019).
79. C. E. Rüter *et al.*, Observation of parity-time symmetry in optics. *Nat. Phys.* **6**, 192–195 (2010).
80. L. Feng *et al.*, Experimental demonstration of a unidirectional reflectionless parity-time metamaterial at optical frequencies. *Nat. Mater.* **12**, 108–113 (2012).
81. L. Feng, R. El-Ganainy, L. Ge, Non-Hermitian photonics based on parity-time symmetry. *Nat. Photon.* **11**, 752–762 (2017).
82. J. Noh *et al.*, Experimental observation of optical Weyl points and Fermi arc-like surface states. *Nat. Phys.* **13**, 611–617 (2017).
83. L. Lu *et al.*, Experimental observation of Weyl points. *Science* **349**, 622–624 (2015).